Coupled Systems Mechanics, *Vol. 11, No. 4 (2022) 315-333*
https://doi.org/10.12989/csm.2022.11.4.315

Investigation of a fiber reinforced polymer composite tube by two way coupling fluid-structure interaction

Fatih Darıcık[1a], Gökhan Canbolat[*1] and Murat Koru[2b]

[1]*Department of Mechanical Engineering, Alanya Alaaddin Keykubat University, Antalya, Türkiye*
[2]*Department of Mechanical Engineering, Isparta University of Applied Sciences, Isparta, Türkiye*

(Received October 16, 2021, Revised April 27, 2022, Accepted May 3, 2022)

Abstract. Fluid-Structure Interaction (FSI) modeling is highly effective to reveal deformations, fatigue failures, and stresses on a solid domain caused by the fluid flow. Mechanical properties of the solid structures and the thermophysical properties of fluids can change under different operating conditions. In this study, we investigated the interaction of $[45/-45]_2$ wounded composite tubes with the fluid flows suddenly pressurized to 5 Bar, 10 Bar, and 15 Bar at the ambient temperatures of 24°C, 66°C, and 82°C, respectively. Numerical analyzes were performed under each temperature and pressure condition and the results were compared depending on the time in a period and along the length of the tube. The main purpose of this study is to present the effects of the variations in fluid characteristics by temperature and pressure on the structural response. The variation of the thermophysical properties of the fluid directly affects the deformation and stress in the material due to the Wall Shear Stress (WSS) generated by the fluid flow. The increase or decrease in WSS directly affected the deformations. Results show that the increase in deformation is more than 50% between 5 Bar and 10 Bar for the same operating condition and it is more than 100% between 5 Bar and 15 Bar by the increase in pressure, as expected in terms of the solid mechanics. In the case of the increase in the temperature of fluid and ambient, the WSS and Von Mises stress decrease while the slight increases of deformations take place on the tube. On the other hand, two-way FSI modeling is needed to observe the effects of hydraulic shock and developing flow on the structural response of composite tubes.

Keywords: computational fluid dynamics, deformation, Fiber Reinforced Polymer Composite (FRPC), fluid-structure interaction, wall shear stress

1. Introduction

The Fluid-structure interaction is a phenomenon associated with fluid systems that causes the deformation and the changes in boundary conditions. This kind of interaction occurs in many natural phenomena and man-made engineering systems. It becomes a crucial consideration in the design and analysis of various engineering systems (Hadzalic *et al*. 2018a, 2018b, Mustafa *et al*. 2021). Therefore, FSI plays an important role in engineering systems due to its multidisciplinary

∗Corresponding author, Ph.D., E-mail: gokhan.canbolat@alanya.edu.tr
[a]Ph.D., E-mail: fatih.daricik@alanya.edu.tr
[b]Associate Professor, E-mail: muratkoru@isparta.edu.tr

http://www.techno-press.org/?journal=csm&subpage=8 ISSN: 2234-2184 (Print), 2234-2192 (Online)

nature. This way, FSI simulations have become more important in the field of multi-physics problems. The one-way coupling is to transfer only the loads calculated with fluid solver into structural domain but the displacement of the structure is also transffered to the fluid solver in two way coupling FS (Boujleben *et al.* 2020).

Fiber Reinforced Polymer Composite (FRPC) tubes have spread usage for transmission of fluids such as clean and wastewater, petroleum and its derivatives, and geothermal fluids. FPRC tubes bring to the fore according to traditional engineering materials owing to the properties of high chemical and corrosion resistance, high specific modulus, and high specific strength (Abdul Majid *et al.* 2011, Hawa *et al.* 2016, Yu *et al.* 2015). The interaction of the flowing fluid and the structure that carries it is an attractive subject for researchers. Characteristics of the flow are the essential parameter that can cause pressure fluctuation-induced vibration and deformations of FRPC tubes. Inlet velocity changes promote the deformation of the tubes (Zhu *et al.* 2014). The material properties of the fluids and the temperature of the medium are also important parameters for the FSI. Enviromental temperature and termal aging effect also mechanical properties of the polymers, such as modulus of elasticity, Poisson's ratio, fracture toughness, etc. (Darıcık *et al*. 2021)

(You and Inaba 2013) investigated the effects of elastic anisotropy on a carbon fiber reinforced plastic (CFRP) thin tube are investigated with FSI. A water pressure wave that causes the deformation of the CFRP tube was generated to investigate coupled fluid-structure motion propagates along the tube and the water. In the experiments, the water-filled CFRP tubes with the winding angles of 45° and 60° have been tested using the impulsive impact to the water, and the histories of strains and pressures have been measured. They concluded that the magnitude of hoop strain by the primary wave decreases with increasing winding angle because the hoop strain is mainly determined by the tube compliance in the breathing mode. (Wang *et al*. 2019) also reported via FSI analysis that during the developing flow, the flow-induced vibration around the hoop of CFRP tube is more intense than the emerging vibration along the tube axis and the damping of the flow direction vibration is more rapid than that of the flow cross vibration (Wang *et al*. 2018). Therefore, the developing flow-induced displacements along the radial direction are significant while the deformations along the tube axis are negligible.

In a study (Zhu *et al*. 2014), FSI is proposed to explore flow erosion and flow-induced deformation of three-limb tubes used in oil transportation based on an FSI method. The main purpose of the study is to investigate the effects of inlet flow rate, diameter ratio of branches and, merging angle of the three-limb tube on the flow characteristics, shear stress distribution, and deformation. They concluded that both flow field and deformation of the tube are important to the structural changes (including the change of branch tube diameter and the change of merging angle) and branch inlet velocity changes.

Higher importing mass flow rate or 90° merging angle can lead to more flow erosion and greater deformation. (Loh *et al.* 2013) performed a FSI simulation was performed in modeling turbulent flow-induced vibration of a curved tube with fixed supports. A two-way FSI simulation method has been used the study the time and frequency response of the curved tube with fixed end supports when subjected to turbulence fluid flow. A flow-induced response test was performed in simulations. The comparison indicates the simulated response is 18.1% higher than the measured response. In a study (Elfaki *et al.* 2021), the effect of changes in crude oil grades on slug characteristics has numerically investigated the influence of changing oil grades and slug characteristics on the maximum induced stresses in horizontal carbon steel tubes. They found that increasing crude oil density causes frequent slugging and promotes the formation of liquid slugs

further upstream near the inlet with high translational velocity and short wavelength.

In the present study, a four-layered FRPC tube that is E-Glass Fabric 7781/SP381 was investigated under different pressure and temperature conditions. Two-way coupling FSI was used to present the changes in deformations and stress over a period. The pressures of 5 Bar, 10 Bar, and 15 Bar were implemented suddenly as the inlet boundary condition for the constant temperatures of 24°C, 66°C, and 82°C for both material and fluid respectively. The effect of changes in the thermophysical properties and the material properties by the temperature on the deformation and stress was analyzed in terms of fluid mechanics and solid mechanics by using two-way coupling FSI. The period of 3 seconds was determined to show the variation of the deformation and stress during the flow in the numerical analyses. The effect of suddenly introducing the pressurized flow as an inlet boundary condition on the structural response is presented for the both beginning and end of the period. Therefore, the results were presented according to 0.05s and 3s of the flow to show the effects of developing flow and the hydraulic shock on structural response.

2. Methodology

In this section, we presented the geometry, generation of mesh, mesh independency tests, boundary conditions, governing equations, and numerical approach.

2.1 Geometry, mesh, and mesh independency test

Fig. 1 shows the four-layer composite tube made of E-Glass Fabric 7781/SP381. The thickness of each layer is 0.25 mm and the total thickness of the composite tube is 1 mm. The diameter of the tube is 30 mm and the length of the tube is 330 mm. The 300 mm hydrodynamic entrance length was provided for the fully developed flow in this turbulent flow (Yunus and Cimbala 2006). The tube is designed with the stacking sequence of $[+45/-45]_2$, fluid mesh for Fluent and structural mesh for transient structural are shown in Fig. 1 numerical analyses performed for a four layered structure.

Fig. 1(a) shows the generated mesh by using Ansys for fluid flow. Triangular elements were used for fluid. Fig. 1(b) shows the generated mesh for the structural domain and structural mesh was used for composite material. Fig. 2 Presents the mesh independency test. An important

Fig. 1 Generated mesh for the tube (a) Fluid flow mesh (b) Structural mesh for composite material

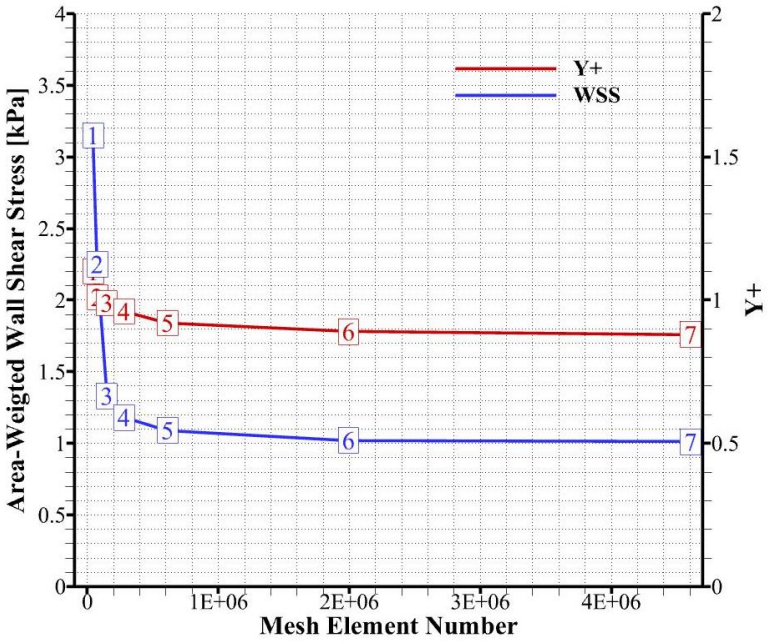

Fig. 2 Mesh sensitivity test

criterion in the mesh dependency tests is the wall y+ value according to the turbulence mode (Canbolat *et al*. 2020). A mesh sensitivity test was performed to determine the sufficient element number according to Area-Weighted Wall Shear Stress (WSS) and Wall Y+ on the wall during the meshing process as in our other studies (Etli *et al*. 2021). The numbers surrounded by a square in Fig. 2. represents the seven different meshes performed analysis separately. Seven different mesh were used by changing element size gradually for numerical calculations. Area-Weighted Wall WSS and Wall Y+ values were investigated by increasing mesh element size and number. According to Decrease in Area-Weighted Wall WSS and Wall is shown in Fig. 2 from mesh number labeled with 1 to mesh number labeled with 7. The numbers surrounded by a square in Fig 2. represents the seven different meshes performed analysis reperately. It appears that the variation in WSS and Y+ started to decrease by the mesh labeled with 5 and it begins to turn into a horizontal line. Therefore, 612325 mesh elements and 2 mm mesh element size were sufficient to perform numerical simulations in Fig. 2. In this way, the computational cost was avoided and sufficient element number was determined. Additionally, the inflation method was used to predict the boundary layer precisely. The inflation is composed of 12 layers to predict to boundary layer development precisely with 1.2 growth rate on the wall in the tube with small diameter.

2.2 Boundary conditions, governing equations, and numerical approach

The flow was incompressible, homogeneous, and fully developed in this study. A No-slip boundary condition was applied to the internal wall in the tube. A fluid-solid interface was defined to the internal wall to reflect the fluid force in the tube The water was used as the fluid in different temperatures and pressures for fluid-structure interaction simulations. Table 1 shows the thermophysical properties of water for 5, 10, and 15 Bar pressures within the 24°C, 66°C, and

Table 1 Thermophysical properties of water

Temperature [°C]	Pressure [Bar]	Density [kg/m^3]	Dynamic Viscosity [Pas]
24°C	5	997.479	0.000910
	10	997.704	0.000910
	15	997.930	0.000910
66°C	5	980.194	0.000427
	10	980.413	0.000427
	15	980.631	0.000427
82°C	5	970.724	0.000345
	10	970.948	0.000345
	15	971.172	0.000346

Table 2 Elastic properties of E-Glass Fabric 7781/SP381 Composite at different ambient temperatures (Tomblin *et al*. 2002)

Temperature (°C)	E_{11} (GPa)	E_{22} (GPa)	E_{33} (GPa)	G_{12} (MPa)	G_{13} (MPa)	G_{32} (MPa)	v_{12}	v_{13}	v_{23}
24	25.06	25.06	10	4.07	3.50	3.50	0.15	0.35	0.35
66	23.61	23.61	8	3.10	2.50	2.50	0.12	0.35	0.35
82	23.92	23.92	9	3.52	3.00	3.00	0.11	0.35	0.35

82°C ambient temperature conditions. 5, 10, and 15 Bar pressure are implemented as the inlet boundary conditions in different ambient temperatures.

Table 2. shows the elastic properties of E-Glass Fabric 7781/SP381 Composite for 5, 10, and 15 Bar pressures within the 24°C, 66 C, and 82°C ambient temperature conditions where E_{11}, E_{22}, and E_{33} are Young modulus in the directions 1, 2, and 3 respectively. G_{12}, G_{13}, and G_{23} are Shear modulus on the planes 12, 13, and 23 respectively. v_{12} is Axial Poisson's ratio and v_{21} is Transverse Poisson's ratio in Table 2.

$$\mathrm{Re} = \frac{\rho \mathrm{U} \mathrm{D_h}}{\mu} \tag{1}$$

Reynolds Number (Re) is defined as the ratio of inertial forces to viscous forces. U, ρ, μ, and D_h are velocity [m/s], density [kg/m^3], dynamic viscosity [Pas], and characteristic length [m], respectively in the Eq. (2). The Re numbers are nearly 35000, 49000, and 60000 for the pressures of 5, 10, and 15 Bar respectively. Re is used to predict the flow whether it is laminar or turbulent flow. It appears that highly turbulent flows occur in-tube flow in this study. In this study, we used two-way coupling FSI therefore ALE approach is used to integrate fluid mechanics and solid mechanics. The equation of Cauchy's law for motion is derived to balance the forces. The product of the velocity and density is balanced with the divergence of the stress tensor and other body forces.

$$\rho \left[\frac{\partial \mathbf{u}}{\partial \mathrm{t}} + \mathbf{u}.\nabla \mathbf{u}\right] = \nabla.\sigma + \mathbf{f} \tag{2}$$

where ρ is the solid density, $\mathbf{u}$ is the velocity vector, $\boldsymbol{\sigma}$ is the Cauchy stress tensor, and f is the external body force. The displacement of the fluid-solid interface and fluid domain is derived from the ALE configuration (Hughes *et al.* 1981).

$$\rho_f \left[\frac{\partial u_f}{\partial t} + u_{\mathbf{f}}.\nabla u_{\mathbf{f}}\right] = -\nabla p + \mu\nabla^2 u_{\mathbf{f}} \quad (3)$$

$$\nabla.\, u_{\mathbf{f}} = 0 \quad (4)$$

where ρ_f is the fluid density, u_f is the velocity vector, μ is the dynamic viscosity, and p is the pressure in the fluid domain.

$$\rho_s \frac{\partial^2 d_s}{dt^2} = \nabla.\sigma_s \quad (5)$$

where d_s is the solid displacement, ρ_s solid density, σ_s is the Cauchy stress in the tube. The forces and velocities must be equal in the fluid-structure interface.

$$u_f = u_s \text{ at the interface of fluid-structure} \quad (6)$$

$$\sigma_s.\, n = \Gamma .n \quad (7)$$

where σ_s is the Cauchy stress tensor, n is the unit normal, and Γ is the real stress. The governing stresses in the wall of the composite tube are planar and the wall thickness is quite low. Therefore, the numerical model was created with the SHELL181 element which has four nodes and six degrees of freedom at each node. The plane stresses in the *k*th orthotropic lamina which has modeled with SHELL181 are defined according to the material coordinate system as

$$\begin{bmatrix}\sigma_1\\ \sigma_2\\ \tau_{12}\end{bmatrix}_k = \begin{bmatrix}Q_{11} & Q_{12} & 0\\ Q_{12} & Q_{22} & 0\\ 0 & 0 & Q_{66}\end{bmatrix}\begin{bmatrix}\varepsilon_1\\ \varepsilon_2\\ \gamma_{12}\end{bmatrix}_k \quad (8)$$

Qij are the stiffness coefficients and also defined below as related to property constants of the material.

$$Q_{11} = \frac{E_1}{1-\nu_{21}\nu_{12}}, \qquad Q_{12} = \frac{\nu_{12}E_2}{1-\nu_{21}\nu_{12}}, Q_{22} = \frac{E_2}{1-\nu_{21}\nu_{12}}, Q_{66} = G_{12}$$

The plane stresses in the kth orthotropic laminar of the laminate can be transformed from the material coordinate system to the global coordinate system via the transformation matrix [T]

$$\begin{bmatrix}\sigma_x\\ \sigma_y\\ \tau_{xy}\end{bmatrix}_k = [T]^{-1}\begin{bmatrix}\sigma_1\\ \sigma_2\\ \tau_{12}\end{bmatrix}_k \quad (9)$$

The transformation matrix [T] is determined with the angle between the material coordinate system and the global coordinate system, *c*=cos(θ), *s*=sine(*θ*).

$$[T] = \begin{bmatrix}c^2 & s^2 & 2sc\\ s^2 & c^2 & -2sc\\ -sc & sc & c^2 - s^2\end{bmatrix} \quad (10)$$

In this study, the SST *k*-*ω* model was used to predict the turbulent flow. Transport equations for the SST *k*-*ω* model

$$\frac{\partial(\rho k)}{\partial t} + \frac{\partial(\rho k u_i)}{\partial x_i} = \frac{\partial}{\partial x_j}\left[\Gamma_k \frac{\partial k}{\partial x_j}\right] + G_k - Y_k + S_k, \quad (11)$$

$$\frac{\partial(\rho\omega)}{\partial t} + \frac{\partial(\rho\omega u_j)}{\partial x_i} = \frac{\partial}{\partial x_j}\left[\Gamma_\omega \frac{\partial\omega}{\partial x_j}\right] + G_\omega - Y_\omega + D_\omega + S_\omega, \quad (12)$$

k and *ω* are the kinetic energy and specific dissipation rate in the SST *k*-*ω* turbulent model. G_k

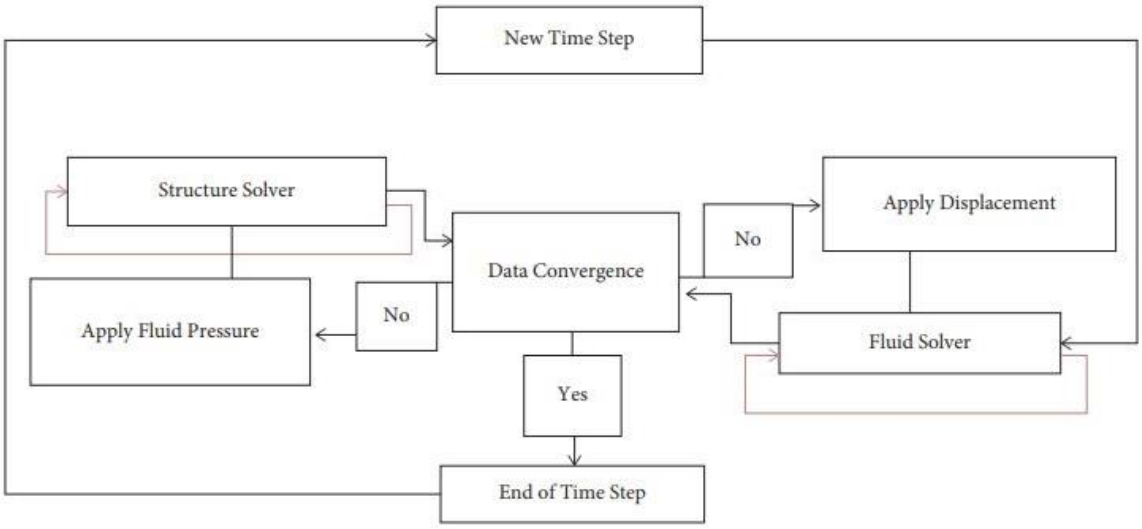

Fig. 3 Flow chart of the two way coupling fluid-structure interaction (Haghani *et al.* 2021)

is defined as the generation of turbulence kinetic energy. G_ω is the generation of ω. Γ_ω and Γ_k are the effective diffusivity of ω and k, respectively. Y_ω and Y_k and are the dissipation of ω and k. S_k and S_ω are user-defined source terms in Equation (10,11) (ANSYS 2013).

The Coupled Pressure-Velocity method was utilized during numerical simulations. The second-order upwind spatial discretization was used to discretize the pressure, momentum, turbulent kinetic energy, and turbulent dissipation rate. The convergence criterion was implemented as 10^{-4} for residuals. The time step size of 0.01s with 300 time steps was used for the transient analyses. 3D flow simulations were performed by the tube seen in Fig. 1. The flow chart of the two-way coupling FSI simulation is shown in Fig. 3. The structure and fluid finite elements are connected directly at the common nodes at the fluid-structure interface (Hadzalic *et al.* 2018).

3. Results and discussion

The parameters such as deformation, wall shear stress, and Von Mises stress are related to both the thermophysical properties of the fluid and elastic properties of the material in a coupled flow-structure analysis. The analysis was performed according to the elastic properties of the structure and thermophysical properties of the fluid at the temperatures of 24°C, 66°C, and 82°C respectively. In this section, the results were presented according to the time and the variations of temperatures under the inlet pressures of 5 Bar, 10 Bar, and 15 Bar respectively. Results were given for a temperature and its 5 Bar, 10 Bar, and 15 Bar operating conditions.

3.1 Results according to flow time

Time-based results were given to present the variation in deformation, wall shear stress, and Von Mises stress in different time steps to investigate the effect of hydraulic shock when the fluid suddenly enters the tube with high pressure. Fig. 4 and Fig. 5 present the results when the fluid

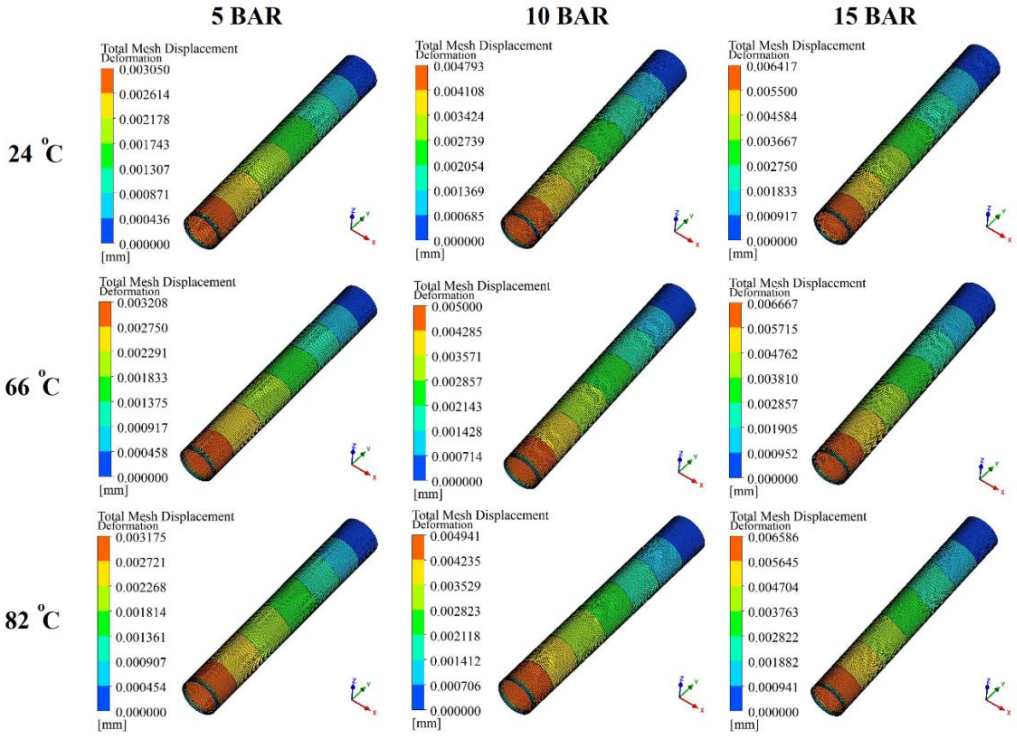

Fig. 4 Deformations when the fluid enters the tube (0.05 s in the period)

enters the tube. Fig. 4 shows the variation of deformation for the beginning of the flow along the tube under the inlet pressure of 5 Bar, 10 Bar, and 15 Bar respectively. As expected, the deformations increased up to two times by the increase in operating pressures from 5 bar to 15 bar. But by comparing the deformations with the change of the temperature it was seen slight variations up to 5.2% increases, take place. When the temperature was increased from 24°C to 82°C, the increase of deformations under 5 bar, 10 bar, 15 bar were 4.1%, 3.1%, and 2.6% respectively. At the beginning of the period, maximum Von Mises stresses in the composite tubes had also little and negligible changes with the increases of the temperature. When the temperature increased from 24°C to 66°C, the decreases of stresses at the tubes under 5 bar, 10 bar, and 15 bar pressure-flows were lower than 1%. The biggest drop of the maximum Von Mises stress with the increase of the temperature from 24°C to 82°C was seen as 2% under the 15 bar pressure flow. The maximum Von Mises stress drops for the tubes under 5 bar and 10 bar with the increase of the temperature from 24°C to 82°C were 0.4% and 1.5% respectively. It is shown that, while the increase in deformations is expected to rise considerably, the increase in deformation and stress is low by an increase in temperature due to variation of thermophysical properties of the fluid. The analyses performed without the FSI could result in lower values for hydrodynamic pressures (Gorman *et al.* 2000) and higher values for the structural values (Heinsbroek 1997) that may lead to large safety margins and unpredictable results in designs (Li *et al.* 2015).

Fig. 6 and Fig. 7, and Fig. 8 present the variations of the total deformation, Von Mises stresses, and WSS according to the flow with the conditions of different pressures and temperatures at the end of the period. As expected, the deformation of the pipe increased in proportion to the increase

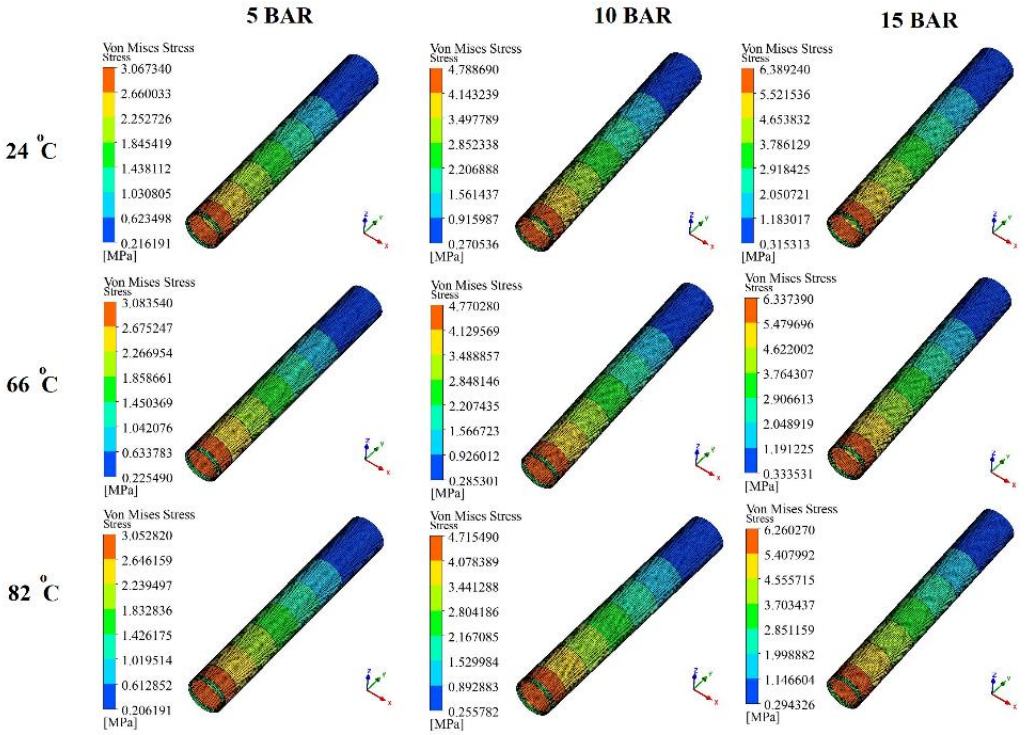

Fig. 5 Von Mises Stress when the fluid enters the tube (0.05 s in the period)

in pressure. By considering the weakening of the E-Glass Fabric 7781/SP381 composite with the rise of ambient temperature it was expected that significant deformations of the tubes could be available. But by comparing the deformations with the change of the temperature it was seen slight variations that correspond to approximately up to 5.8% reductions, take place. When the temperature was increased from 24°C to 82°C, the increase of deformations under 5 bar, 10 bar, and 15 bar were 5.8%, 5.3%, and 5.2% respectively. However, the deformations at the time of 5 bar pressure-flow entering the tube are just about three times more than the deformations at the end of the period for each temperature condition. The deformations at the time of 10 bar pressure-flow and 15 bar pressure-flow entering the tube are just about two times more than the deformations at the end of the period for each temperature condition. This is related to hydraulic shock when the fluid suddenly enters the tube at high pressure. Hydraulic shock is defined as a non-stationary flow when pressure changes correspond to sudden changes of flow velocities (Bureček *et al.* 2015). The hydraulic shock occurs due to a change in the initial velocity of liquid flow. Positive or negative abrupt liquid acceleration in a pipe can lead to excessive deformations and failures (Hružík *et al.* 2014).

At the end of the period, 5 bar, 10 bar, and 15 bar pressure-flow induced maximum Von Mises stresses in the composite tubes had significant and similar changes with the increases of the temperature. When the temperature increased from 24°C to 66°C, the decreases of stresses at the tubes under 5 bar, 10 bar, and 15 bar pressure flows were 8.4%, 8.01%, and 7.8% respectively. The biggest drop of the maximum Von Mises stress with the increase of the temperature from 24°C to 82°C was seen as 11.1% under the 15 bar pressure flow. The maximum Von Mises stress

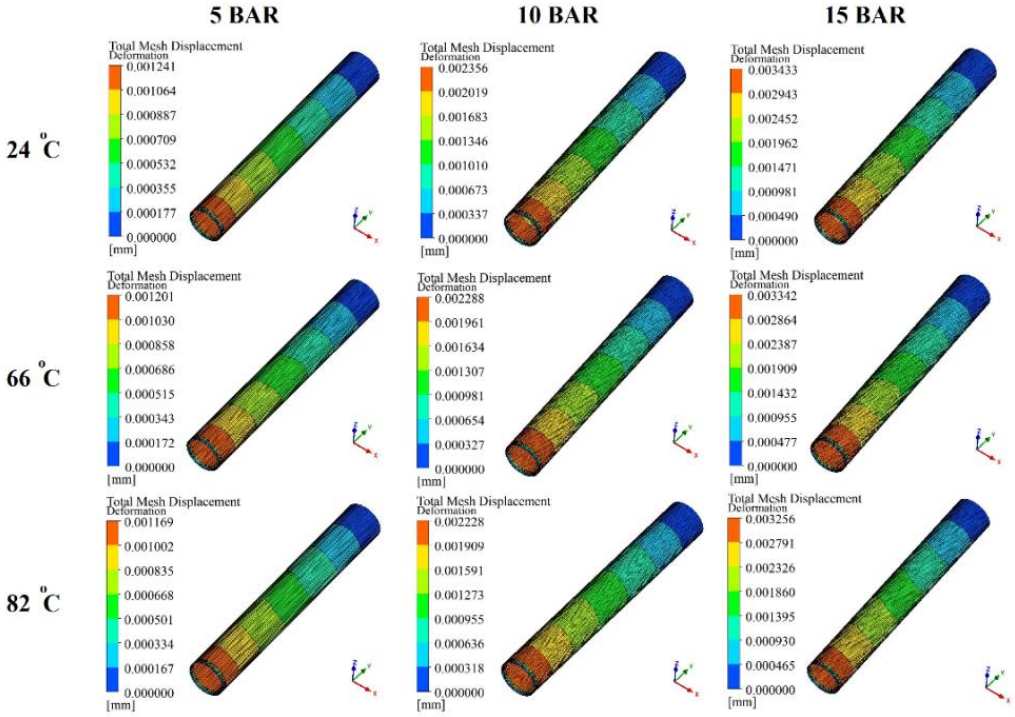

Fig. 6 Deformations at the end of the period (3s in the period)

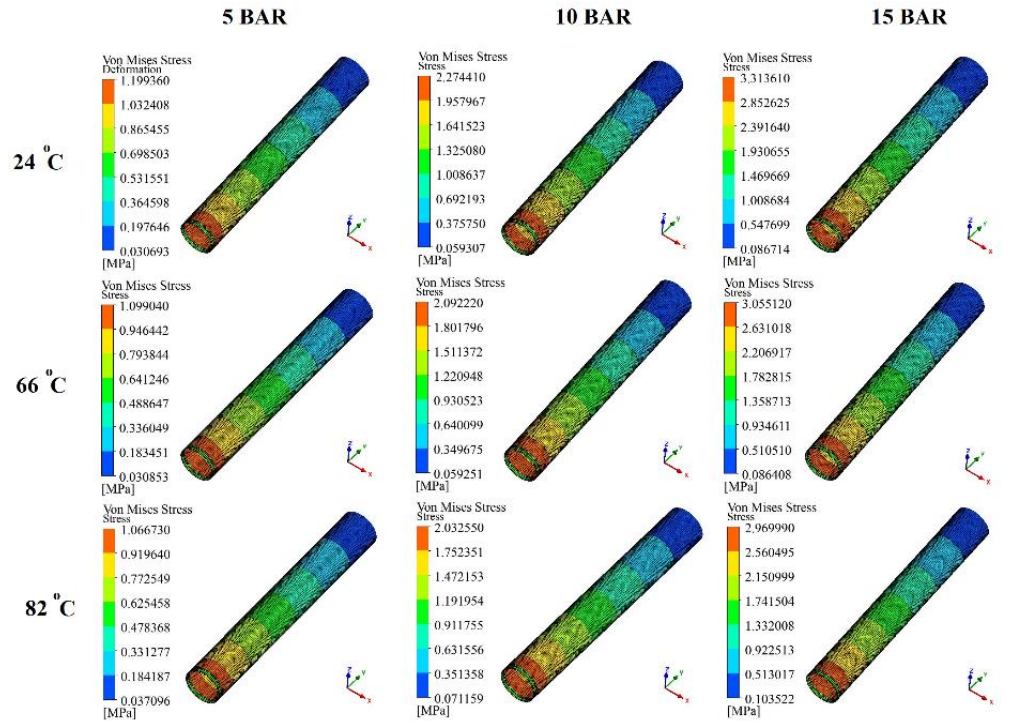

Fig. 7 Von Mises Stress at the end of the period (3s in the period)

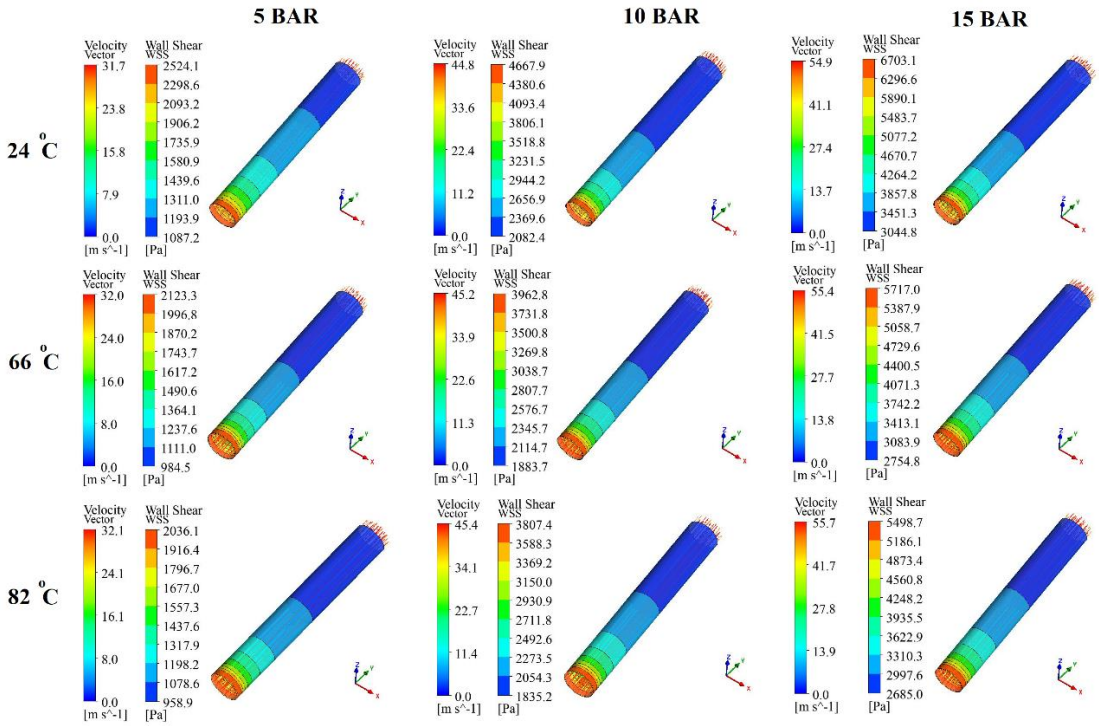

Fig. 8 Wall Shear Stress and Velocity Vectors at the end of the period

drops for the tubes under 5 bar and 10 bar with the increase of the temperature from 24°C to 82°C were 10.6% and 10.4%. By comparing the variations of the stresses during the period, it was observed that because of the hydraulic shock, tubes were stressed more than two times at the inlet period according to the end period.

In this study, the variations in deformation and stress at the beginning of the period are significantly high according to the end of the period. When fluid enters the tube, deformations and stress are two times more than the end of the period because hydraulic shock is dominant. The fluid enters the tube suddenly with high pressure and it combines with the developing flow effect, so deformations and stress are considerably high at the beginning of the period.

Fig. 8 shows the WSS and velocity contours of these flows. It is seen that WSS increases by the increase in pressure in each case. However, the decrease in the viscosity by the increase in the temperature directly affects the WSS values in this flow as in Fig. 8. The fluid velocity reaches 31.7 m/s, 44.8 m/s, and 54.9 m/s for the temperature of 24°C. It reaches 32 m/s, 45.2 m/s, and 55.4 m/s for the temperature of 66°C. In the last case of 82°C, it reaches 32.1 m/s, 45.4 m/s, and 55.7 m/s under the 5 Bar, 10 Bar, and 15 Bar respectively in Fig. 8. The Reynolds number of the cases is higher than 10^6, therefore a turbulent flow occurs in the tube. The differences in the velocity under the same pressure occur due to variation of the fluid viscosity with temperature. When the results are investigated for the WSS at 24°C, the maximum WSS values are 2524 Pa, 4667 Pa, and 6703 Pa under the 5 Bar, 10 Bar, and 15 Bar respectively in Fig. 8. The WSS are 2123 Pa, 3962 Pa, and 5717 Pa under the 5 Bar, 10 Bar, and 15 Bar for the 66°C and they are 2036 Pa, 3807 Pa, and 5498 Pa for the 82°C respectively.

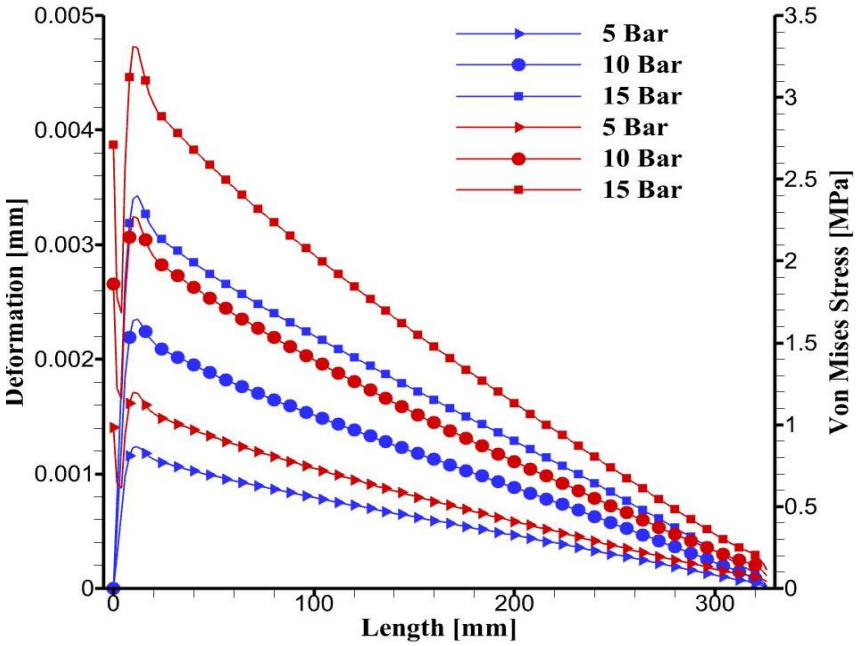

Fig. 9 Deformations and Von Mises Stress along the wall of tube at 24°C

3.2 Temperature-based results along the tube

In this section, the results were given along the wall of the tube. The variation of deformation, Von Mises stress, and WSS were given in a line on the wall at the temperatures of 24°C, 66°C, and 82°C. The blue line, red line, and green line represent the deformation, Von Mises stress, and WSS respectively. Fig. 9 and Fig. 10 show the results for the 24°C. Fig. 11 and Fig. 12 show the results for 66°C. Fig. 14 and Fig. 15 show the results for the 82°C.

Fig. 9 and Fig. 10 show the variation of deformation, Von Mises stress, and WSS along the wall of the tube at the end of the period for the temperature of 24°C. As shown in Fig. 9. that deformations and Von Mises stress are highly different between the inlet and end of the pipe.

The deformation of 1.23 μm is the maximum value at the entrance region and it is almost 0.01 μm at the end of the pipe when the fully developed flow occurs for the operating conditions of 24°C and 5 Bar in Fig. 9. The maximum and minimum Von Mises stress values are 1.198 MPa and 0.040 MPa at the entrance region and the beginning of fully developed flow respectively for the operating conditions of 24°C and 5 Bar. The maximum and minimum WSS values are 2.522 kPa and 1.140 kPa at the entrance region for the operating conditions of 24°C and 5 Bar in Fig. 10.

The deformation of 2.35 μm is the maximum value at the entrance region and it is almost 0.03 μm at the end of the pipe when the fully developed flow occurs for the operating conditions of 2°C and 10 Bar in Fig. 9. The maximum and minimum Von Mises stress values are 2.270 MPa and 0.100 MPa at the entrance region and the beginning of fully developed flow respectively for the operating conditions of 24°C and 10 Bar. The maximum and minimum WSS values are 4.660 kPa and 2.190 kPa at the entrance region and fully developed flow region respectively for the operating conditions of 24°C and 10 Bar in Fig. 10.

The deformation of 3.42 μm is the maximum value at the entrance region and it is almost 0.05

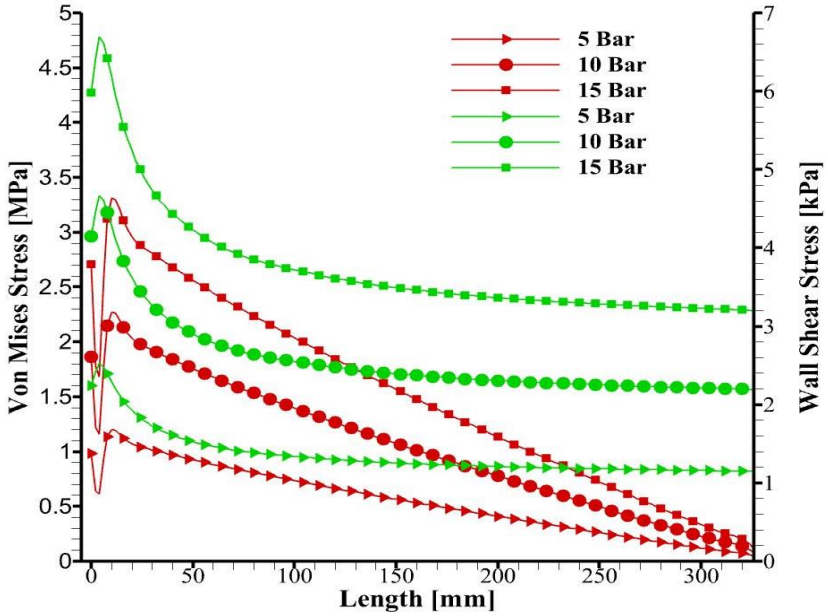

Fig. 10 Von Mises Stress and Wall Shear Stress along the wall of tube at 24°C

μm at the end of the pipe when the fully developed flow occurs for the operating conditions of 24°C and 15 Bar in Fig. 9. The maximum and minimum Von Mises stress values are 3.310 MPa and 0.150 MPa at the entrance region and the beginning of fully developed flow respectively for the operating conditions of 24°C and 15 Bar. The maximum and minimum WSS values are 6,690 kPa and 3.20 kPa at the entrance region and the beginning of fully developed flow respectively for the operating conditions of 24°C and 15 Bar in Fig. 10.

Fig. 11 and Fig. 12 show the variation of deformation, Von Mises stress, and WSS along the wall of the tube at the end of the period for the temperature of 66°C.

The deformation of 1.19 μm is the maximum value at the entrance region and it is almost 0.007 µm at the end of the pipe when the fully developed flow occurs for the operating conditions of 66°C and 5 Bar in Fig. 9. The maximum and minimum Von Mises stress values are 1.090 MPa and 0.039 MPa at the entrance region and the beginning of fully developed flow respectively for the operating conditions of 66°C and 5 Bar. The maximum and minimum WSS values are 2.120 kPa and 1.030 kPa at the entrance region and fully developed flow region respectively for the operating conditions of 66°C and 5 Bar in Fig. 10.

The deformation of 2.23 μm is the maximum value at the entrance region and it is almost 0.014 µm at the end of the pipe when the fully developed flow occurs for the operating conditions of 66°C and 10 Bar in Fig. 9. The maximum and minimum Von Mises stress values are 2.090 MPa and 0.102 MPa at the entrance region and the beginning of fully developed flow respectively for the operating conditions of 66°C and 10 Bar. The maximum and minimum WSS values are 3.950 kPa and 1.970 kPa MPa at the entrance region and fully developed flow region respectively for the operating conditions of 66°C and 10 Bar in Fig. 10. The deformation of 3.30 μm is the maximum value at the entrance region and it is almost 0.057 μm at the end of the pipe when the fully developed flow occurs for the operating conditions of 66°C and 15 Bar in Fig. 9. The maximum and minimum Von Mises stress values are 3.050 MPa and 0.145 MPa at the entrance region and

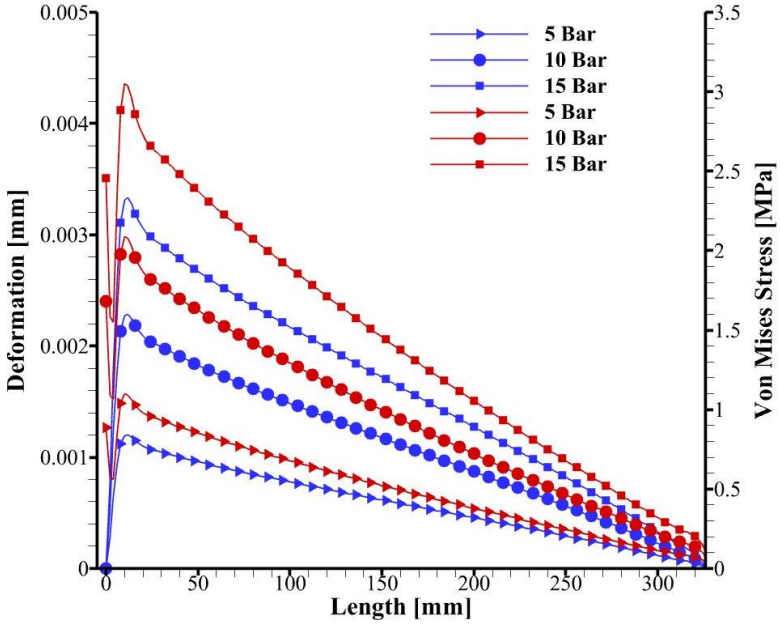

Fig. 11 Deformations and Von Mises Stress along the wall of tube at 66°C

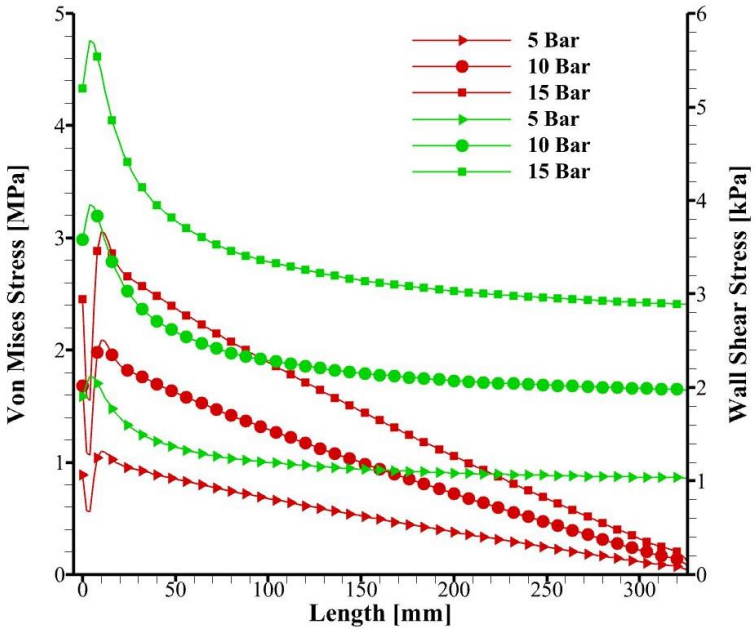

Fig. 12 Von Mises Stress and Wall Shear Stress along the wall of tube at 66 °C

the beginning of fully developed flow respectively for the operating conditions of 66°C and 15 Bar. The maximum and minimum WSS values are 5.700 kPa and 2.880 kPa MPa at the entrance region and fully developed flow region respectively for the operating conditions of 66°C and 15 Bar in Fig. 10.

Fig. 11 and Fig. 12 show the variation of deformation, Von Mises stress, and WSS along the wall of the tube at the end of the period for the temperature of 82°C.

The deformation of 1.19 μm is the maximum value at the entrance region and it is almost 0.008 μm at the end of the pipe when the fully developed flow occurs for the operating conditions of 82°C and 5 Bar in Fig. 9. The maximum and minimum Von Mises stress values are 1.050 MPa and 0.041 MPa at the entrance region and the beginning of fully developed flow respectively for the operating conditions of 82°C and 5 Bar. The maximum and minimum WSS values are 2.010 kPa and 1.000 kPa at the entrance region and the beginning of fully developed flow respectively for the operating conditions of 82°C and 5 Bar in Fig. 10.

The deformation of 2.10 μm is the maximum value at the entrance region and it is almost 0.0015 μm at the end of the pipe when the fully developed flow occurs for the operating conditions of 82°C and 10 Bar in Fig. 9. The maximum and minimum Von Mises stress values are 2.010 MPa and 0.108 MPa at the entrance region and the beginning of fully developed flow respectively for the operating conditions of 82°C and 10 Bar. The maximum and minimum WSS values are 3.570 kPa and 1.920 kPa MPa at the entrance region and the beginning of fully developed flow respectively for the operating conditions of 82°C and 10 Bar in Fig. 10.

The deformation of 3.20 μm is the maximum value at the entrance region and it is almost 0.022 μm at the end of the pipe when the fully developed flow occurs for the operating conditions of 82°C and 15 Bar in Fig. 9. The maximum and minimum Von Mises stress values are 2.950 MPa and 0.120 MPa at the entrance region and the beginning of fully developed flow respectively for the operating conditions of 82°C and 15 Bar. The maximum and minimum WSS values are 5.340 kPa and 2.810 kPa MPa at the entrance region and the beginning of fully developed flow respectively for the operating conditions of 82°C and 15 Bar in Fig. 10.

Fig. 13 shows the pressure drop in pipe flow. As mentioned above, deformations, stress, and WSS values decrease along the tube due to developing flow. For all operating conditions, similar results were presented in the figures.

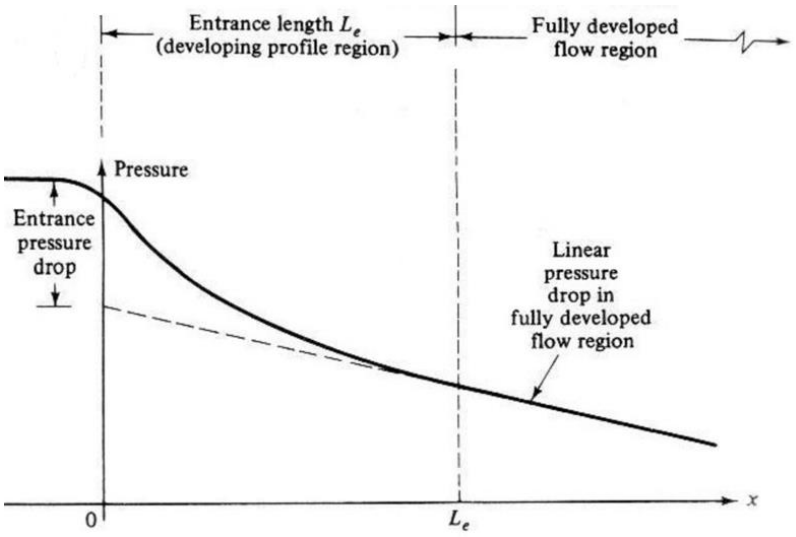

Fig. 13 Developing flow (Munson *et al.* 2013)

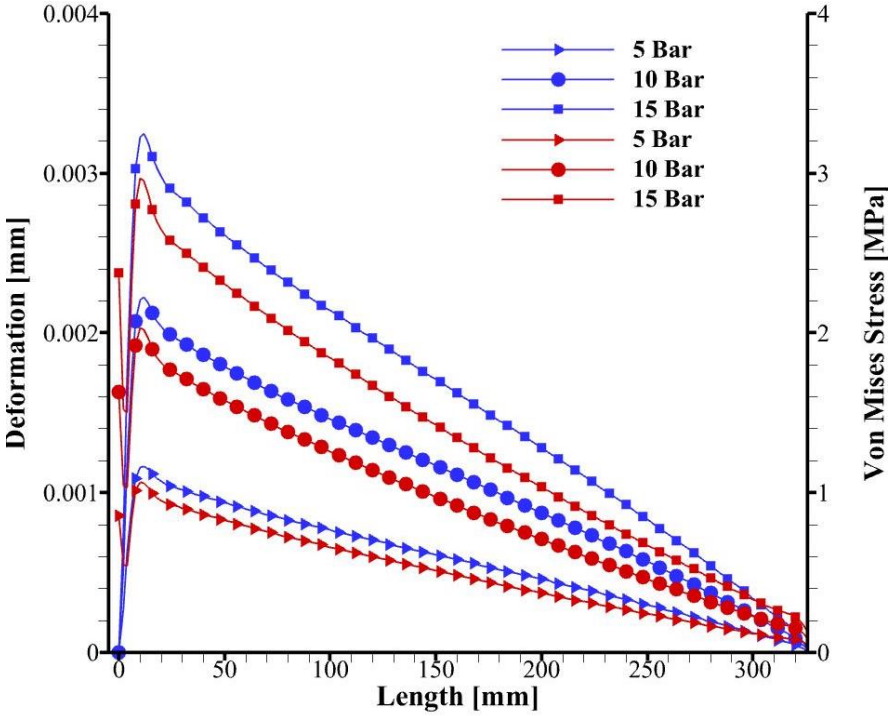

Fig. 14 Deformations and Von Mises Stress along the wall of tube at 82°C

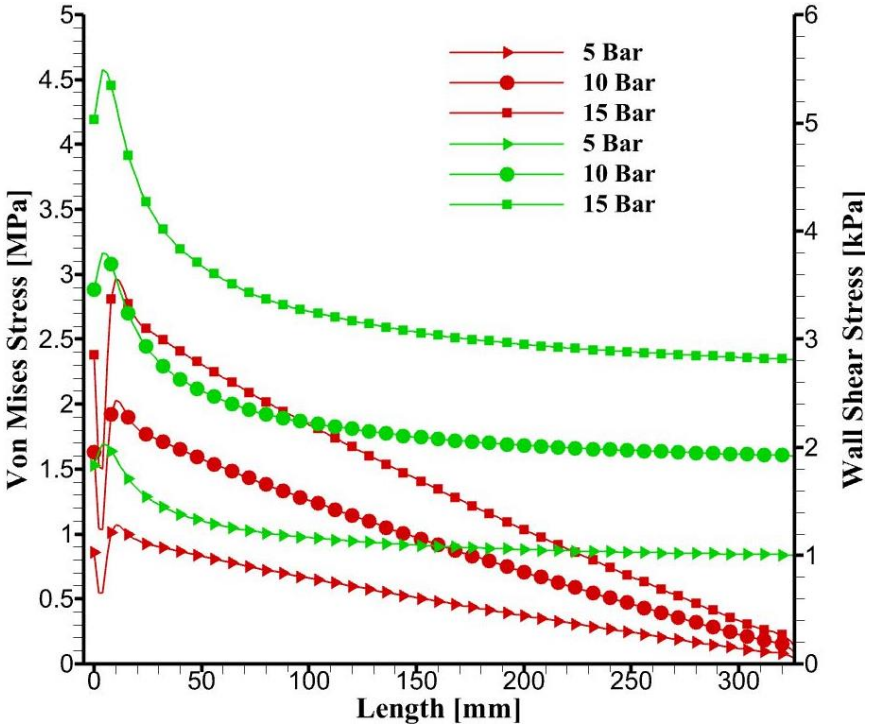

Fig. 15 Von Mises Stress and Wall Shear Stress along the wall of tube at 82°C

4. Conclusions

This study provides a coupled mechanics perspective for pressurized sudden flow in a Fiber Reinforced Polymer Composite. An FRPC tube was investigated under different operating conditions in terms of fluid mechanics and solid mechanics by fluid sturucture interaction. Transient analyses were performed to show developing flow and hydraulic shock effects in the pipe flow when sudden pressurized to 5 Bar, 10 Bar, and 15 Bar within the temperatures of 24°C, 66°C, and 82°C. Therefore, the unsteady flow was solved with a period of 3 seconds in the numerical analysis. The water was used as the fluid in this study, that's why the density of the fluid can be negligible under the pressure implemented in this study. However, the change in the temperature of the fluid and environment directly affect the viscosity of the fluid so the decrease in the fluid viscosity changes the WSS on the wall. Considering the results, the following conclusions were reached:

- When the structural response of the FPRC tube was compared for all temperature and pressure conditions implemented in this study, developing flow significantly increases the deformations and Von Mises stress than that of the fully developed flow.
- Developing flow induces two times higher WSS than the developed flow-induced WSS for all temperature and pressure conditions.
- While the weakening of elastic properties of FPRC with the rise of temperature can cause significant deformations on the tubes in solid mechanics, it was observed that the decrease in the fluid viscosity provides compensation for the excessive deformation.
- The FRPC tubes were stressed and deformed at the initiation of the period nearly two times more than at the end of the period due to the hydraulic shock has occurred at the beginning of the flow, for all temperature and pressure conditions.
- Two-way coupling FSI analyses are necessary to observe the effects of variation in thermophysical properties of the fluid on structural response.

References

ANSYS (2013), Ansys Fluent Theory Guide, PA, 15317.

Boujleben, A., Ibrahimbegovic, A. and Lefrançois, E. (2020), "An efficient computational model for fluid-structure interaction in application to large overall motion of wind turbine with flexible blades", *Appl. Math. Model.*, **77**, 392-407. https://doi.org/10.1016/j.apm.2019.07.033.

Munson, B.R., Young, D.F. and Okiishi, T.H. (1995), "Fundamentals of fluid mechanics", *Oceanograph. Literat. Rev.*, **10**(42), 831.

Bureček, A., Hružík, L. and Vašina, M. (2015), "Simulation of accumulator influence on hydraulic shock in long pipe", *Manuf. Indus. Eng.*, **14**(1-2), 1-4. https://doi.org/10.12776/mie.v14i1-2.461.

Canbolat, G., Yildizeli, A., Köse, H.A. and Çadirci, S. (2020), "Numerical investigation of hydrodynamic and thermal boundary layer flows over a flat plate and transition control", *Int. J. Adv. Eng. Pure Sci.*, **32**(4), 390-397. https://doi.org/10.7240/jeps.636786.

Çengel, Y.A. and Cimbala, J.M. (2006), *Fluid Mechanics Fundamentals and Applications*, HillHigher Education, Boston.

Darıcık, F., Delibaş, H., Canbolat, G. and Topcu, A. (2021), "Effects of short-term thermal aging on the fracture behavior of 3D-printed polymers", *J. Mater. Eng. Perform.*, **30**(12), 8851-8858. https://doi.org/10.1007/s11665-021-06374-z.

Elfaki, M., Nasif, M.S. and Muhammad, M. (2021), "Effect of changing crude oil grade on slug characteristics and flow induced mechanical stresses in pipes", *Appl. Sci.*, **11**(11), 5215.

https://doi.org/10.3390/app11115215.
Etli, M., Canbolat, G., Karahan, O. and Koru, M. (2021), "Numerical investigation of patient-specific thoracic aortic aneurysms and comparison with normal subject via Computational Fluid Dynamics (CFD)", *Med. Biolog. Eng. Comput.*, **59**(1), 71-84. https://doi.org/10.1007/s11517-020-02287-6.
Gorman, D.G., Reese, J.M. and Zhang, Y.L. (2000), "Vibration of a flexible pipe conveying viscous pulsating fluid flow", *J. Sound Vib.*, **230**(2), 379-392. https://doi.org/10.1006/jsvi.1999.2607.
Hadzalic, E., Ibrahimbegovic, A. and Dolarevic, S. (2018a), "Failure mechanisms in coupled soil-foundation systems", *Couple. Syst. Mech.*, **7**(1), 27-42. https://doi.org/10.12989/csm.2018.7.1.027.
Hadzalic, E., Ibrahimbegovic, A. and Dolarevic, S. (2018b), "Fluid-structure interaction system predicting both internal pore pressure and outside hydrodynamic pressure", *Couple. Syst. Mech.*, **7**(6), 649-668. https://doi.org/10.12989/csm.2018.7.6.649.
Haghani, A., Jahangiri, M., Yadollahi Farsani, R., Khosravi Farsani, A. and Fazilatmanesh, J. (2021), "Transient fluid-solid interaction and heat transfer in a cavity with elastic baffles mounted on the sidewalls", *Math. Prob. Eng.*, **2021**, Article ID 8842898. https://doi.org/10.1155/2021/8842898.
Hawa, A., Majid, M.A., Afendi, M., Marzuki, H.F.A., Amin, N.A.M., Mat, F. and Gibson, A.G. (2016), "Burst strength and impact behaviour of hydrothermally aged glass Fibre/Epoxy composite pipes", *Mater. Des.*, **89**, 455-464. https://doi.org/10.1016/j.matdes.2015.09.082.
Heinsbroek, A.G.T.J. (1997), "Fluid-structure interaction in non-rigid pipeline systems", *Nucl. Eng. Des.*, **172**(1-2), 123-135. https://doi.org/10.1016/s0029-5493(96)01363-5.
Hružík, L., Bureček, A. and Vašina, M. (2014), "Non-stationary flow of hydraulic oil in long pipe", *EPJ Web Conf.*, **67**, 1-5. https://doi.org/10.1051/epjconf/20146702042.
Hughes, T.J., Liu, W.K. and Zimmermann, T.K. (1981), "Lagrangian-Eulerian finite element formulation for incompressible viscous flows", *Comput. Meth. Appl. Mech. Eng.*, **29**(3), 329-349. https://doi.org/10.1016/0045-7825(81)90049-9.
Li, S., Karney, B.W. and Liu, G. (2015), "FSI research in pipeline systems-A review of the literature", *J. Fluid. Struct.*, **57**, 277-297. https://doi.org/10.1016/j.jfluidstructs.2015.06.020.
Loh, S.K., Faris, W.F. and Hamdi, M. (2013), "Fluid-structure interaction simulation of transient turbulent flow in a curved tube with fixed supports using LES", *Prog. Comput. Fluid Dyn.*, **13**(1), 11-19. https://doi.org/10.1504/PCFD.2013.050646.
Majid, M.A., Assaleh, T.A., Gibson, A.G., Hale, J.M., Fahrer, A., Rookus, C.A.P. and Hekman, M. (2011), "Ultimate Elastic Wall Stress (UEWS) Test of Glass Fibre Reinforced Epoxy (GRE) pipe", *Compos. Part A: Appl. Sci. Manuf.*, **42**(10), 1500-1508. https://doi.org/10.1016/j.compositesa.2011.07.001.
Mustafa, M.A., Abdullah, A.R., Hasan, W.K., Habeeb, L.J. and Nassar, M.F. (2021), "Two-way fluid-structure interaction study of twisted tape insert in a circular tube having integral fins with nanofluid", *East.-Eur. J. Enterp. Technol.*, **3**, 25-34. https://doi.org/10.15587/1729-4061.2021.234125.
Tomblin, J., Sherraden, J., Seneviratne, W. and Raju, K.S. (2002), "Advanced general aviation transport experiments. A–Basis and B–Basis design allowables for epoxy–based prepreg Toray T700GC-12K-31E/# 2510 unidirectional tape", National Institute for Aviation Research Wichita State University, Wichita, Kansas, 23.
Wang, C., Ge, S., Sun, M., Jia, Z. and Han, B. (2019), "Comparative study of vortex-induced vibration of FRP composite risers with large length to diameter ratio under different environmental situations", *Appl. Sci.*, **9**(3), 517. https://doi.org/10.3390/app9030517.
Wang, C., Sun, M., Shankar, K., Xing, S. and Zhang, L. (2018), "CFD simulation of vortex induced vibration for FRP composite riser with different modeling methods", *Appl. Sci.*, **8**(5), 1-18. https://doi.org/10.3390/app8050684.
You, J.H. and Inaba, K. (2013), "Fluid-structure interaction in water-filled thin pipes of anisotropic composite materials", *J. Fluid. Struct.*, **36**, 162-173. https://doi.org/10.1016/j.jfluidstructs.2012.08.010.
Yu, K., Morozov, E.V., Ashraf, M.A. and Shankar, K. (2015), "Numerical analysis of the mechanical behaviour of reinforced thermoplastic pipes under combined external pressure and bending", Composite Structures, **131**, 453-461. https://doi.org/10.1016/j.compstruct.2015.05.033.
Zhu, H., Zhang, W., Feng, G. and Qi, X. (2014), "Fluid-structure interaction computational analysis of flow

field, shear stress distribution and deformation of three-limb pipe", *Eng. Fail. Anal.*, **42**, 252-262. https://doi.org/10.1016/j.engfailanal.2014.04.021.

AI